Peculiarities of Climate Change in Central Africa

Check for updates

Mamy Magbini Tokpa and V. A. Lobanov

Abstract The multiyear series of mean monthly air temperatures at 65 meteorological stations in Central Africa are considered to assess the influence of climate change on the dynamics of multiyear mean values. Due to the spatial and temporal heterogeneity of observations, a methodology based on a sequential transition from more reliable to less reliable information, the assessment of the stability of nonstationarity indicators, the selection of areas homogeneous in climate change dynamics, and the quantification of the changes occurred depending on the type of mean value change and on the choice of effective climate models was developed. As a result, we received quantitative estimations of air temperature growth in different seasons, which reach 2.2–2.4 °C in southern mountainous and eastern regions in all seasons and summer monsoon in the coastal areas and spring intermonsoon period in the north. In the central part of the territory, the growth of average temperatures does not exceed 0.5–0.6 °C. Efficient climate models were also selected for the territory for the forthcoming assessment of future temperature.

Keywords Mean monthly temperature · Climate change · Central Africa · Multiyear series modeling · Temperature growth estimates

1 Introduction

Climate change is one of humanity's significant challenges in the twenty-first century [1, 2]. Its impact is now evident in all sectors of public and private activity [3]. The IPCC (Intergovernmental Panel on Climate Change), in its 5th Assessment Report, states that global warming is unequivocally characterized by an increase in the average temperature of the atmosphere and oceans [4]. Moreover, the air temperature increases differently in different latitudes, and the most significant temperature increase was observed in temperate latitudes and the south of Siberia [5]. Based on the latitudinal growth of albedo from the equator to the poles, according to physical

M. M. Tokpa (✉) · V. A. Lobanov
Russian State Hydrometeorological University, St. Petersburg, Russia
e-mail: mtmamy2013@gmail.com; rshu@rshu.ru

and mathematical models of climate in the modern warming, one should expect the greatest temperature increase in high latitudes and the smallest in low or equatorial latitudes, which includes the territory of Central Africa considered in this paper. However, in the IPCC reports, the temperature increase in equatorial regions of Africa is highly uncertain, ranging from 0.2 to 2 °C, mainly due to the low reliability of the observational data [6–10].

According to the average scenarios presented in the 5th IPCC report and confirmed by various other climate studies, large areas of Africa will warm more than 2 °C above pre-industrial levels this century [11, 12]. Temperature increases in regions of Africa, including Central Africa, are expected to be higher even than global average temperature increases (by 1.5 and 2 °C), and heat waves are expected to be more frequent and prolonged. Temperature extremes in this region are expected to be higher than the global average, with the most intense warming occurring in the Sahel [13–17]. Several studies have found that trees in the Congo Basin in Central Africa are losing their ability to absorb carbon dioxide, which may lead to an additional increase in temperature [18, 19].

Due to the high uncertainty of the results obtained for the Central African region, this work aims to comprehensively evaluate the quality of the observational data and the estimates of temperature change in this region using statistical methods and models.

2 Climatic Regime of the Territory and Baseline Data

In the present work, we consider the territory of Central Africa, where 65 weather stations with the longest series of observations of average monthly air temperatures were selected (Fig. 1).

The analysis of spatial temperature changes during the year for the considered territory shows the following main situations of its dynamics. In January, relatively low temperatures are observed throughout the region (up to a maximum of 25–27 °C near the Gulf of Guinea), with their lowest values in the northeast and the mountainous southeastern part (20–22 °C) of the territory compared to the center. This situation is due to the influence of the winter phase of the African monsoon, in which the cool and dry air of North Africa moves southward following the movement of the Inter-Tropical Convergence Zone (ITCZ). Then, due to the growth of incoming radiation, the whole area warms up, reaching maximum temperatures in March–April, especially in the northern part (up to 32–33 °C). By summer, the second phase of the African monsoon begins with a shift of the ITCZ to the Northern Hemisphere and a shift of humid Atlantic air following it. The presence of cloudiness and somewhat cooler air from the ocean leads to an overall decrease in temperatures, which is especially noticeable in the western and southwestern parts of the area near the Gulf of Guinea, where temperatures become the same as in the mountainous southeastern part (20–22 °C). In autumn, there is natural radiative heating of the territory during the intermonsoon period, with maximum temperatures in the northern part near the
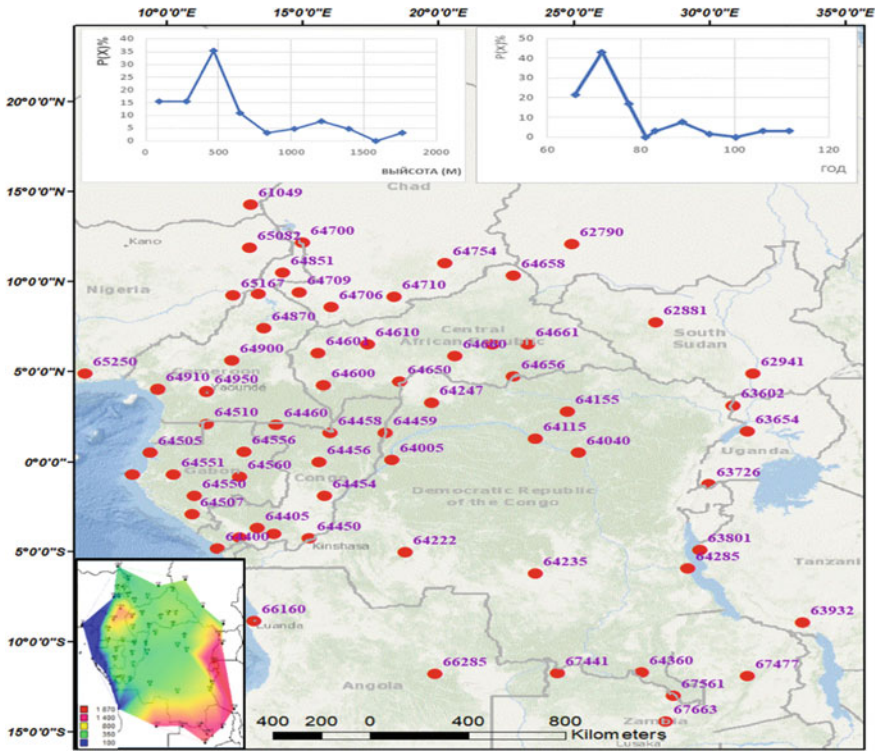
Fig. 1 The map-scheme of weather stations and with small diagrams the distribution of stations by the duration of the series of observations, by height and a map of altitude of station

Sahel (up to 27–28 °C) and minimum temperatures in the mountainous areas (21–22 °C). Temperature variations across the territory range from 7–10 °C in winter to 12–13 °C in April.

In general, it should be noted that throughout the year winter, spring and summer are colder in the mountains and on the sea coast, and spring and summer are warmer in the north than in other parts of the region. As a result, the natural variability (root-mean-square deviation—RMSD) throughout the territory is less than 1 °C, except for the north of the territory in winter and spring and the south in summer and autumn, where the RMSD is slightly greater than 1 °C.

For formalized evaluation of homogeneity and data quality, we applied the statistical criteria of Dixon and Smirnov-Grabbs to evaluate the homogeneity of extremes of empirical distributions and Fisher and Student statistical criteria to evaluate stationarity of dispersions and mean values of two identical parts of the time series [20–22].

As a result, the observation sites were divided into two groups according to the quality of information and duration: 30 sites with long and continuous observation series and the remaining sites with short observation series, unreliable and heterogeneous data, and missing observations.

The methodology based on the construction of regression dependences for the joint period between the short observational series and the longer ones at the reference points has been applied to bring the short observational series to the multiyear period and restore the missing observations [23, 24].

3   Research Methodology

Research methodology is based on approximation of multiyear time series by non-stationary mean models of two types: linear trend and step changes of mean values with an estimation of efficiency of these models in relation to stationary sampling model and modeling itself are described in detail in papers [25–29]. In this case, to assess the effectiveness of the models, such an indicator as the mean square deviation (RMSD) of the model residuals σ_ε is used, and the smaller it is, the better the model is. Moreover, RMSD of the residuals is related to the coefficient of determination of the model (R^2) by the following functional relation:

$$\sigma_\varepsilon = \sigma_y \sqrt{1 - R^2}, \tag{1}$$

where σ_y is the standard deviation of the original series, characterizing the natural variability.

Obviously, for the stationary sample model $\sigma_\varepsilon = \sigma_y$ and $R^2 = 0$. If a nonstationary mean model is more efficient than a stationary sample model, then its $\sigma_\varepsilon < \sigma_y$. Therefore, the relative difference $\Delta = (\sigma_y - \sigma_\varepsilon)/\sigma_y$. Expressed in % can be a measure of the efficiency of any nonstationary mean model. As a first approximation, we can assume that if $\Delta > 10\%$, the nonstationary mean model is more efficient than the stationary mean model. The statistically significant difference between the nonstationary mean model and the stationary model can also be estimated based on the Fisher criterion by comparing the calculated value $F = \sigma_y^2/\sigma_\varepsilon^2$ with the critical F_{cr} at a given significance level α and sample size n [22]. In work [30], the formula connecting Δ and F_{cr} at $\alpha = 5\%$ is given. Thus, at $n = 120$, $F_{cr} = 1.35$ and $\Delta = 13.8\%$, and at $n = 60$, $F_{cr} = 1.53$ and $\Delta = 19.4\%$. When approximating the time series by the step change model of the average, the year of transition from one stationary condition to another is also determined by iterations when reaching the minimum of the sum of squares of deviations from each mean of two parts of the series—$T_{ст}$.

4 Results and Discussion

4.1 Patterns Obtained Based on Long Series

First, modeling was carried out, and the stability of model parameters was evaluated for the 30 longest series with reliable observational data. The results in the form of average values of the efficiency parameters of nonstationary models r, $\Delta_{\text{тр}}$, $\Delta_{\text{ст}}$, and $T_{\text{ст}}$ are given in Table 1 for two parts of the longest time series: from the beginning of observations until 1960 and from 1961 to 2021.

Table 1 shows that all the nonstationarity in the temperature series occurs after 1960, i.e., in the last period since the second half of the twentieth century. The nonstationarity indices $\Delta_{\text{тр}}$ and $\Delta_{\text{ст}}$ are on average >10% for temperatures in all months of the year, with maximum values of 18–20% in July–September. At the same time, in all cases, $\Delta_{\text{ст}} > \Delta_{\text{тр}}$ (on average after 1960 $\Delta_{\text{тр}} = 11.8\%$, $\Delta_{\text{ст}} = 16.4\%$), indicating greater efficiency of the nonstationary model of step changes in the average than the linear trend model in the approximation of time series. On average, the year of such step transitions from one stationary condition to another belongs to the late 1980s and early 1990s. The correlation coefficients r of air temperature with time for all months are statistically insignificant.

Table 1 Results of estimation of stability of model parameters for 30 longest series

Months	$\Delta_{\text{тр}}$		$\Delta_{\text{ст}}$		r		$T_{\text{ст}}$	
	Before 1960	After 1960	Before 1960	After 1960	Before 1960	After 1960	Before 1960	After 1960
1	7.0	10.0	1.1	13.2	0.06	0.29	1948	1994
2	8.8	10.9	0.8	14.3	0.13	0.35	1946	1995
3	9.9	11	1.5	15.1	0.08	0.39	1948	1995
4	8.9	10.6	1.1	14.7	0.13	0.33	1947	1988
5	7.2	10.3	1.3	15.9	0.09	0.33	1947	1987
6	9.2	11.9	0.1	15.7	0.24	0.4	1946	1991
7	7.0	16.6	0.5	20.4	0.18	0.48	1948	1992
8	6.2	13.9	1.0	18.2	0.08	0.41	1946	1991
9	5.7	12.4	0.3	18.0	0.03	0.35	1945	1991
10	7.2	11.0	0.2	17.6	0.04	0.31	1941	1988
11	9.1	13.0	1.1	18.1	0.02	0.38	1945	1994
12	7.8	10	1.0	15.2	0.1	0.3	1948	1992

4.2 Spatial and Temporal Patterns of the Indicators of Nonstationary Models

For the longest observational series, it was found that all changes occurred in the second half of the twentieth century and, on average, in the late 1980s and early 1990s. Therefore, the observational series only from 1960 was considered for modeling at the remaining sites. As a result, the efficiency parameters of nonstationary models r, $\Delta_{\text{тр}}$, $\Delta_{\text{ст}}$ and the years of transition from one quasi-stationary regime to another $T_{\text{ст}}$ were calculated for all observation points and for all average monthly temperatures of the year. Figure 2 shows spatial distributions of correlation coefficients r of mean monthly temperatures with time for all months of the year, which allow us to estimate the evolution of the areas of nonstationary models. With the series duration of 61 years (1961–2021), statistically significant r starts from $r = 0.32$, and therefore second and third gradations of r in Fig. 2 will represent regions of nonstationary mean models.

An analysis of the dynamics of such regions of nonstationary patterns during the year allows us to draw the following conclusions. During the winter monsoon, areas of nonstationary patterns arise along the borders of the territory, occupying about 50% of its total area with a maximum of nonstationarity in February in the east. During the summer monsoon, when humid, warm air masses come from the Atlantic, the area of nonstationary patterns, especially in July and August, occupies up to 2/3 of the total area under consideration and also covers the western coastal regions. During the autumn intermonsoon period, the area of nonstationary patterns gradually decreases and shifts from west to east, comprising only 36% of the total
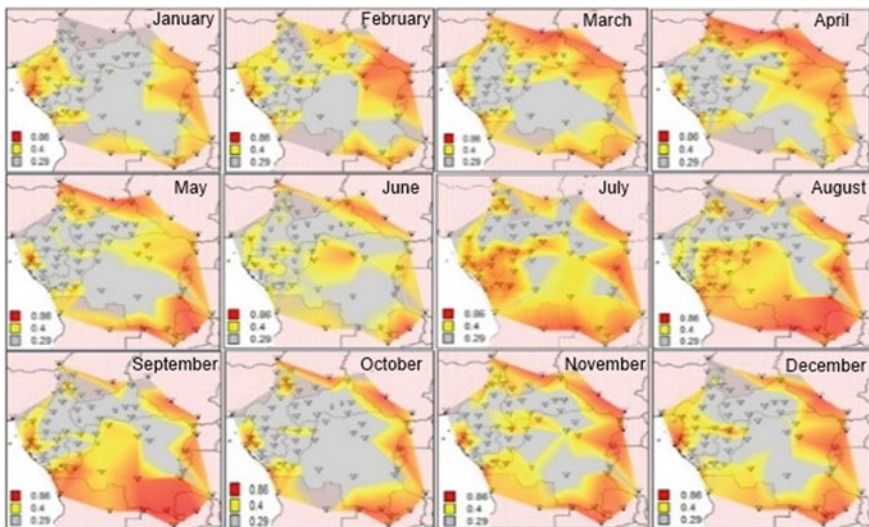

Fig. 2 Spatial distributions of correlation coefficients (r) of air temperature over time during the year

area in October. In general, nonstationary patterns are observed throughout the year in the eastern and southeastern parts of the territory and, as a rule, in the mountainous regions.

4.3   Area Zoning by Type of Climatic Change

Since the model of step changes in average temperature values proved more effective than the trend model, it is necessary to establish the years of step-growth of temperatures and quantify changes in average values. Figure 3 shows that these years vary within a wide range: from the mid-1970s to the early 2000s. At the same time, they are grouped by areas and allow to identify areas homogeneous by type of climate change. In addition, it was found that there may be one-step transition in the multiyear temperature series in some cases, while in others, there may be two.

In addition to T_{cT}, the correlation radius obtained based on the constructed spatial correlation functions of air temperatures for each month was also used as an additional attribute of zoning [22, 30]. As a result, 4 homogeneous areas were singled out according to the dynamics of changes in the average air temperature value; thus, in
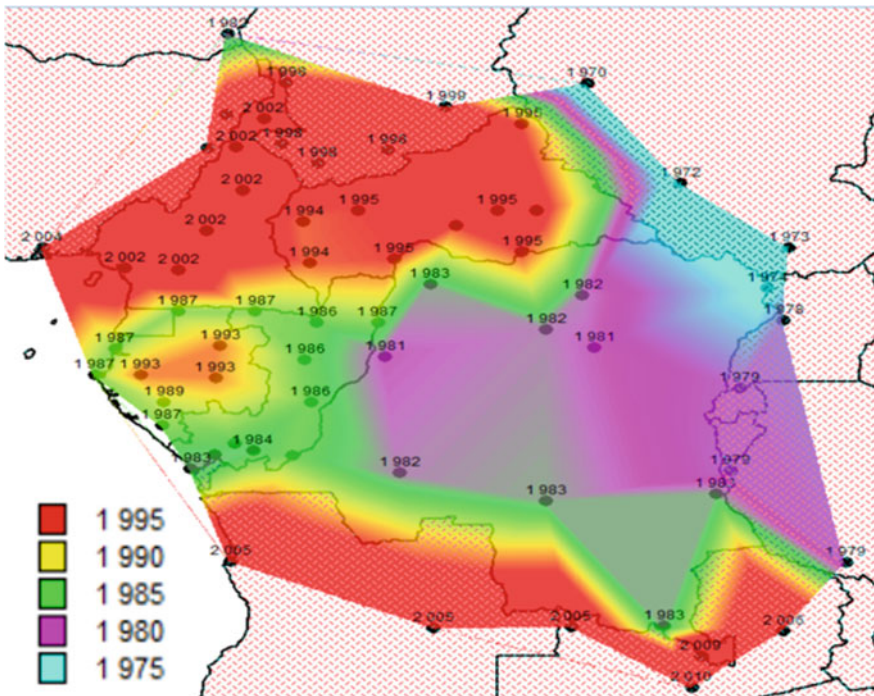

Fig. 3 Spatial distribution of years of transition from one stationary condition to another

the western coastal area № 1 there was a one-step increase in the average temperature in 2002, and the average change $\Delta t_{\mathrm{cp}} = 0.7$ °C. In the southern mountainous area № 2, there were two-step increases in temperature in 1984 and in 2002, and each temperature rise was about 0.5 °C. In area № 3, covering the central and eastern parts of the territory, also has two increases in average temperatures in 1977 and 1997, totaling 0.7 °C. In the northern area № 4, there is only one step change in the mean value in 1996, amounting to 0.7 °C.

After developing the classification, its effectiveness should be evaluated, for example, by calculating and comparing the correlation coefficients between the average series in each area and the observation series in all weather stations of the territory in question [31].

4.4   Quantification of Temperature Growth

Quantitative assessment of temperature growth is based on the model view for each period before and after the established year of step changes $T_{\mathrm{cт}}$. If there is a stationary average model for each part of the time series, then the quantification of temperature growth is defined as the difference between the average of the two parts of the time series: $\Delta t_{\mathrm{cp}} = t_{\mathrm{cp2}} - t_{\mathrm{cp1}}$, где t_{cp1}, t_{cp2} are the average temperatures of the first and second parts of the series.

To assess the stationarity of each of the two parts of the time series, correlation coefficients r with time were calculated, which turned out to be statistically insignificant in the vast majority of cases. Therefore, the average series in homogeneous regions and each temperature series at weather stations Δt_{cp} were determined. For the average series in homogeneous areas, it was found that Δt_{cp} varies by 0.7 °C in winter, by 1.2 °C in spring, from 0.8 to 1.0 °C in summer, and from 0.8 to 1.2 °C in fall. However, whether these changes are significant or not can be assessed only by comparing them with natural climatic variability, which is quantitatively expressed by the standard deviation (RMSD) of the whole multiyear series. If the changes in the mean value exceed the RMSD, we can consider them significant. According to the rule of three-sigma for the normal distribution law, a twofold excess of RMSD corresponds to the reliability of concluding the statistical significance of the obtained changes with a probability of 95%. If the obtained changes of average values in areas for different seasons of the year are presented in fractions of RMSD, they would be 0.6 RMSD in winter, 0.9–1.1 in spring, 1.0–1.3 in summer, and 1.1–1.4 RMSD in autumn. Thus, changes in mean multiyear temperatures in summer and autumn are more significant than in spring and winter in relation to their natural climatic variability.

Of course, of the greatest interest are the spatial changes obtained both in Δt_{cp} themselves at the stations and in relation to the RMSD. Examples of such spatial variations of mean long-term temperatures are shown in Fig. 4 for temperatures of mean months of all year seasons, and in relation to RMSD in Fig. 5.
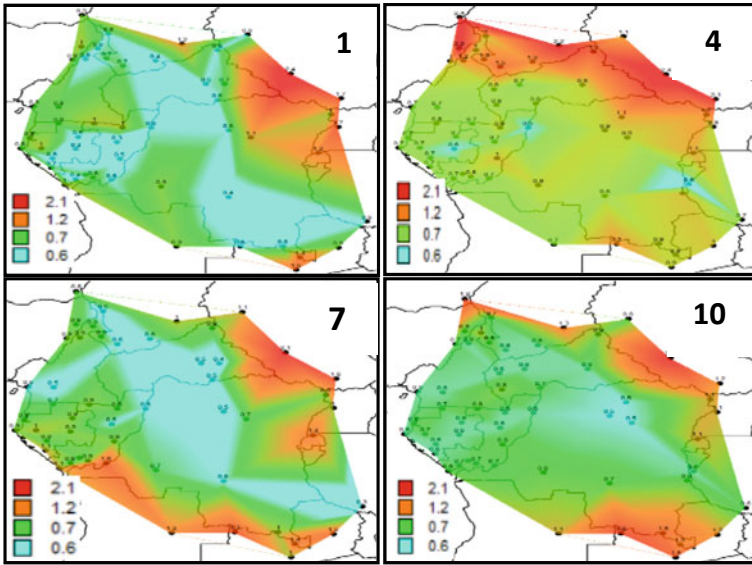
Fig. 4 Spatial distributions of the growth of average long-term temperatures in the middle months of the seasons of the year
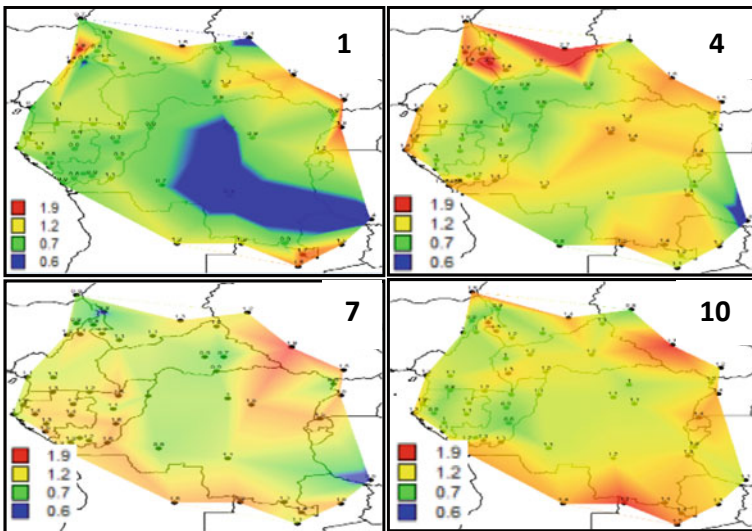

Fig. 5 Spatial distributions of the growth of average long-term temperatures in the middle months of the seasons of the year in fractions of standard deviations

It follows from Fig. 4 that during the winter monsoon (January), the most significant temperature increases of 1–2 °C occurred in the east and south in the mountains, The smallest temperature increases of 0.5 °C was observed in the central part, and, in the north and in the western coastal areas the temperature increase was 0.6–1.2 °C. During the inter-monsoon spring period (April), the most significant increase in mean multiyear temperatures to 2.2–2.4 °C was observed in the north. It was associated with increased desertification and expansion of the Sahara, and a shift of the Sahel to the south. Over the rest of the territory, the temperature increase ranged from 0.6 to 0.9 °C, with slightly higher values of up to 1.2 °C in the southern mountainous part. During the summer monsoon (July), the greatest temperature increase to 1.8–2.2 °C is observed in the east, and another band of significant temperature increases to 1.0–1.6 °C occurs in the southern mountainous part and in the western coastal part. The increase in the central part of the tropical forests was not more than 0.5–0.6 °C. During the intermonsoon fall period (October), the greatest increase was from 1.1 to 2.1 °C in the northeast and in the southern highlands. In the central part, the increase was also up to 0.5–0.6 °C.

Thus, in all seasons there are two parts of the territory with high temperature growth (the southern mountainous and eastern regions) and the central area of tropical forests, where the temperature growth is almost always (except for the hot spring season) small. In the summer monsoon, the coastal area is also added to the area of high-temperature increase due to the air masses from the central Atlantic, where the ocean surface temperature (OST) increases. And in the hot spring inter-monsoon period, the northern part is added, where the influence of the Sahara moving from the north is already felt.

If we consider Δt_{cp} in relation to RMSD (Fig. 5), the highest excess of RMSD from 1.1 to 1.7–2.1 occurs during intermonsoon periods (spring and autumn). It covers up to 90% of the area, with maximums also in the north and in the mountainous southern region. In January, during the winter monsoon, the multiyear variability is large and the Δt_{cp}/RMSD ratio reaches a maximum of 1.7–1.8, with Δt_{cp}/RMSD < 1 for half of the area and <0.5–0.6 in the central region. In July during the summer monsoon, the Δt_{cp}/RMSD ratio is approximately the same for the entire area and averages 1.2–1.3.

4.5 Selection of Effective Climate Model for Central Africa

The main research tools, especially for future climate change assessment, are physical and mathematical models of the general atmosphere and ocean circulation (GAOC), which already number more than 50 within CMIP5/CMIP6 projects [32, 33]. These models have different resolutions (number of grid nodes by latitude and longitude and levels by altitude in the atmosphere and depth in the ocean) and different climate characterization schemes in explicit constructions and parameterization on the intra-grid scale [34–36]. As a result, there is uncertainty both in reconstructing today's climate from different climate models and even greater uncertainty in estimating projections

into the future until the end of the twenty-first century. On the other hand, climate models are based on regularities of general atmosphere and ocean circulation. They do not always effectively take into account regional climatic features of a specific territory, for example, extremely hot (Arabian Peninsula) or cold (Sakha Republic (Yakutia)) conditions [33, 34]. Therefore, the main task for assessing current and especially future regional climate changes is choosing the most effective climatic model when comparing modeling and observational data for a specific territory.

The following models were chosen as competing climate models, which have information on the results of ongoing experiments on the CMIP5 project freely available on the Internet [10]:

1. Hadley Centre for Climate Prediction, Met Office, UK, HadCM3 Model.
2. Institute for Numerical Mathematics, Russia, INM CM4.0 Model.
3. Model of the Max Planck Institute for Meteorology, Germany (ECHAM5/MPI OM).
4. The Beijing Climate Center, China, BCC Model.
5. IPSL/LMD/LSCE, France, CM4 V1 model.
6. Meteo-France, Centre National de Recherches Meteorologiques, CNRM, CM3 Model.
7. Bjerknes Centre for Climate Research, Norway, BNU-ESM, BCM2.0 Model.
8. Canadian Centre for Climate Modelling and Analysis, CanESM2, CGCM3.1 Model, T63 resolution.
9. The Japanese high-resolution MIROC3.2 model (CCSR/NIES/FRCGC, Japan, MIROC3.2, high resolution), MIROC-ESM.

The methodology for choosing an effective model is based on comparing the observational data and the data from the historical experiment (Historical experiment 1850–2005) for a joint period. 30 year duration, emphasizing the correspondence of the averages for the last observation period, e.g. 1976–2005. Obviously, those models which show the smallest deviation from the multiyear average of the observational data are the most efficient. Therefore, four-time periods were selected: 1950–1975, 1961–1990 (the period recommended by WMO), 1976–2005, and 1950–2005 and the average air temperatures in typical months of all seasons: January, April, July, October.

4.6 Comparison of Simulation and Observation Data for Different Periods

First, we calculated the differences between the mean multiyear temperatures for the entire joint period between the simulated and observed values. The results of these differences ($\Delta = T_{mod} - T_{obs}$) averaged over all 65 weather stations for each month of the year are shown in Table 2.

The data in Table 2 show that the average modulo differences (Δ) range from 2.0 to 5.5 °C, and on average, for all months, the smallest differences for the three models

Table 2 Differences between modeled and observed multiyear average temperatures for all weather stations in Central Africa

| Months	Climate models										
	Cmcc-cm	CNRM	Hadley	INM	IPSL–CM5A-MR	Micro5	MPI	NorESM1-M	BCC
1	2.3	2.2	2.5	3.4	2.0	2.3	2.6	2.8	2.1
2	3.1	3.1	2.7	4.7	2.6	2.7	3.3	3.6	2.8
3	4.0	4.1	3.4	5.4	3.4	3.2	4.0	4.5	3.6
4	4.1	4.2	3.7	5.5	3.5	3.8	4.3	4.7	3.8
5	3.9	4.0	3.6	5.1	3.4	3.7	4.1	4.4	3.6
6	3.6	3.6	3.9	4.2	3.5	3.5	3.8	3.8	3.2
7	3.4	3.4	3.7	4.0	3.3	3.3	3.8	3.3	2.9
8	2.5	2.7	3.1	3.5	2.7	2.8	2.9	2.7	2.5
9	2.7	2.8	2.9	4.1	2.3	2.5	3.0	3.0	2.4
10	2.7	2.7	2.8	4.1	2.3	2.6	2.9	3.1	2.6
11	2.5	2.5	2.7	3.8	2.2	2.3	2.7	2.9	2.3
12	2.6	2.6	3.0	3.5	2.3	2.5	2.8	2.9	2.4
среднее	3.1	3.2	3.2	4.3	**2.8**	**2.9**	3.4	3.5	**2.9**
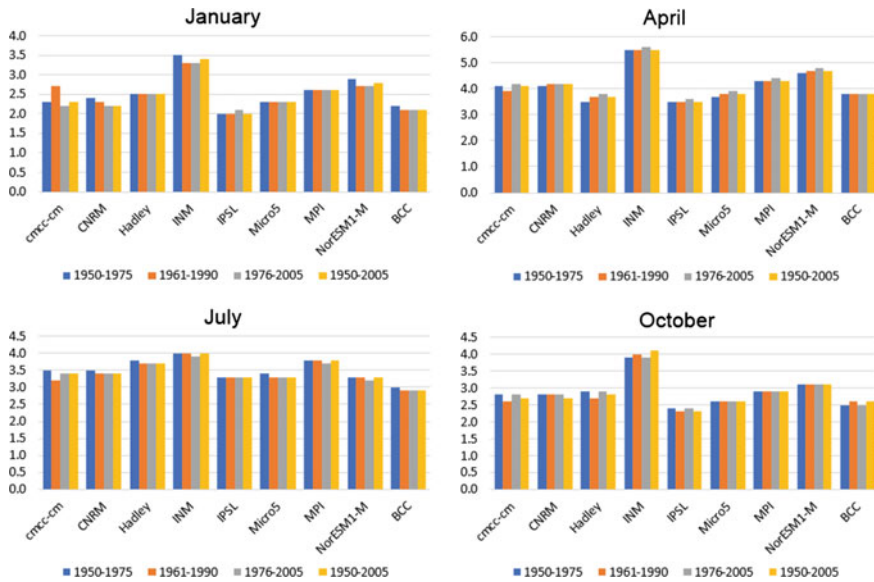
Fig. 6 Differences between modelled and observed mean multiyear temperatures at weather stations in Central Africa

are 2.8–2.9 °C. However, even these smallest (Δ) exceed the natural variability (RMSD), which ranges from 0.6 °C in September to 0.9 °C in January on average for the area, by several times.

Figure 6 shows the differences in the mean multiyear temperatures (modulo) between the simulated and observed data on average for the entire territory of Central Africa for different periods and characteristic months of all year seasons.

Based on the obtained diagrams, we can conclude that the modulo average error is almost independent of the given averaging periods and varies from 2 to 5.5 °C depending on the climate model and season of the year. The smallest errors were obtained using two climate models: IPSL (French Laplace Institute model) and BCC (Beijing Climate Center model, China). The average territorial errors of these models range from 2 °C in autumn and winter to 2–3 °C in spring and summer. For this territory, such errors are significant because they exceed the standard deviation of natural multiyear fluctuations (RMSD) by 2 or more times, which should be considered when adjusting especially the future climate projections.

4.7   Estimation of Errors by Territory

The selected most effective IPSL, and BCC models have the smallest error but average for the whole territory and modulo. At the same time, the spatial distribution of these errors can be heterogeneous both in magnitude and in sign. Therefore, spatial
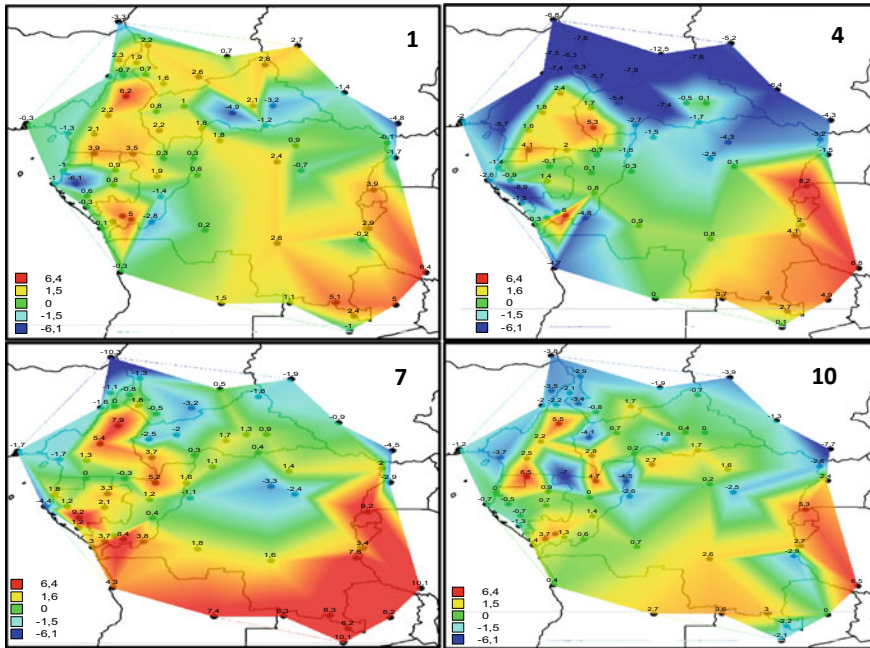
Fig. 7 Spatial distributions of systematic errors of the IPSL model for air temperature in characteristic months (month numbers) of the year

distributions of errors over Central Africa were plotted and analyzed, shown for the IPSL model and characteristic months of all seasons of the year in Fig. 7, and the BCC model in Fig. 8. The differences in the multiyear mean values were considered only for the last 30 year period from 1976 to 2005. Figure 6 shows that these differences practically do not depend on the considered period, and the last period is the closest to the subsequent extrapolation by climate scenarios.

The spatial distributions of the systematic errors of the IPSL model indicate that in winter (January), the deviations are mostly positive and reach their maximum values (up to +6.4 °C) in the southeast, where the mountains are located. A similar situation of local maximum positive errors in the northwest, where mountainous areas are also located. Such a large systematic overestimation of the model data is due to the fact that the historical experiment considered only the surface temperature at sea level. Therefore, in the mountainous regions, either model data at other vertical levels should be taken into account, or a large positive correction for the vertical temperature gradient should be introduced. Negative errors with local maxima of −4 to −6 °C occur near the coast and in the interior of tropical forests. In these areas, the actual temperature is higher than that calculated by the model, which is associated with the heat effect of the Gulf of Guinea and equatorial forests in the winter and cool phase of the African monsoon. In spring (April), during the hottest inter-monsoon period, the distribution of errors is more differentiated: large negative
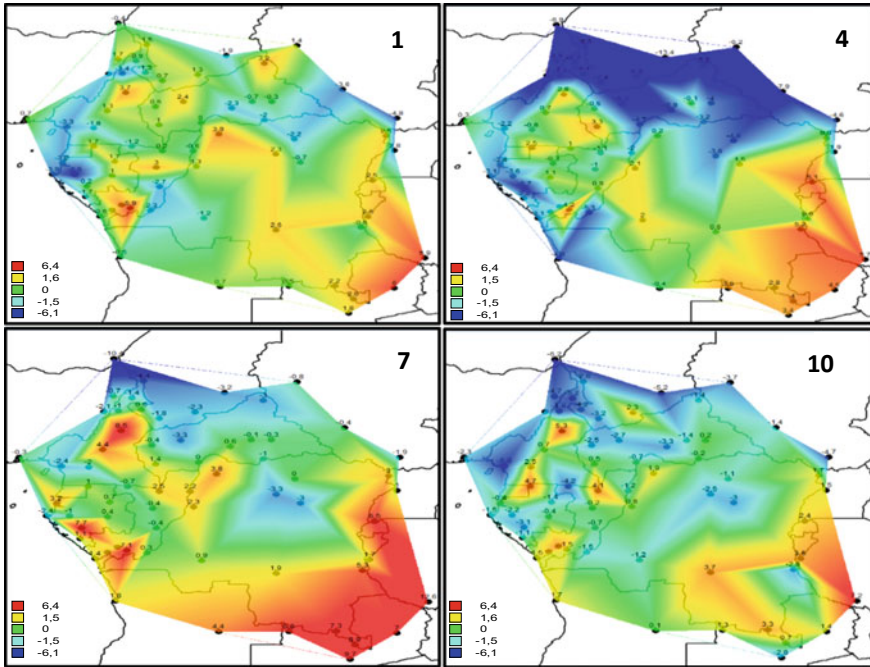
Fig. 8 Spatial distributions of systematic errors of the BCC model for air temperature in characteristic months (month numbers) of the year

errors (up to −12 °C) in the north and large positive errors (up to +6.8 °C) in the south in the mountain regions. The actual temperature in the north is higher than the calculated one due to considerable warming of the territory and the influence of hot air in the Sahel and the Sahara. In summer (July), during the summer phase of the African monsoon, a similar division of territory by errors is preserved, but in the southern mountainous areas, the deviations are larger (up to +8 to +10 °C), and in the northern areas smaller (down to −8 °C). In autumn (October) during the intermonsoon period, the spatial distribution of errors is more homogeneous, and their marginal values are smaller. Thus, in the north, negative errors practically do not exceed −3 ÷ −4 °C (although there are two local extremes to −7 °C), and in mountainous areas (northwest and south), errors do not exceed +6.5 °C. In some local cases, large deviations from model data can also be caused by large errors in the observational data.

During all seasons of the year in Fig. 8, the largest positive deviations take place in the southern mountainous regions (from +4 to +5 °C in winter to +10 ÷ +12 °C in summer), and the largest negative deviations are observed in the northern regions and the gulf coast also throughout the year with the highest values up to −10 ÷ −12 °C in spring and with the lowest −4 ÷ −6 °C in autumn and winter. In the winter period (January), positive temperature differences (up to +6 °C) occur in the

center, northeast, and southeast of the territory in question, and negative values (up to −6.6 °C)—in the extreme west, northeast, and central south. In the spring period (April), positive differences (up to +5.7 °C) are observed in the southeast, and east, and negative values (up to −13.4 °C) occur from the sea coast in the southwest to the north and northeast. In summer (July), positive temperature differences (up to +12.6 °C) are observed over most of the territory with the highest values in the volcanic region of Cameroon and shifted from the west coast to the south and east. Negative values (from −10.4 °C) are located from the extreme west to the north to the center. In the autumn period (October), the largest temperature differences up to +7.2 °C are observed in the southeast and east, and negative values up to −6.2 °C and more are located in the far west, north, and northeast.

5 Conclusions

In particular, the following conclusions were obtained.

1. The observational data are highly heterogeneous in time and space, with the most unreliable observations occurring in the Democratic Republic of Congo, which occupies nearly half Central Africa.
2. A methodology was developed and applied to estimate climatic changes in air temperature in Central Africa, based on a sequential transition from more reliable to less reliable information, an assessment of the stability of no stationarity indicators, on the identification of areas homogeneous in climate change dynamics and on the quantification of changes that have occurred, depending on the type of mean value change model.
3. It is established that changes in average value took place in the second half of the twentieth century, from the middle of 1970 to the beginning of 2000, and the model of stepped changes in average value is more effective than the trend model.
4. On the territory of Central Africa, four areas homogeneous in the dynamics of changes in the mean value were identified, and in two of them, the step temperature rise occurred twice: the first in the late 1970s—early 1980s and the second in the late 1990s—early 2000s, and in the remaining two once: in the mid-1990s or early 2000s.
5. In all seasons, the southern mountainous, and eastern regions of the territory had the highest temperature rise to 2.0–2.2 °C, which is 1.7–2.1 RMSD. In the summer monsoon, the western coastal strip is also added to the area of high temperature rise to 1.5–1.7 °C due to humid and warm air masses from the Atlantic, where OST increases. Another area of high-temperature increases in the north up to 2.2–2.4 °C occurred during the hottest spring intermonsoon period and is apparently related to the Saharan advance southward. In the central part of the territory, where there are tropical forests, the temperature increase in almost

all seasons (except spring) is small and does not exceed 0.5–0.6 °C, which is less than RMSD.

6. The French IPSL model of the Laplace Institute and the Chinese BCC model of the Beijing Climate Center proved to be the most efficient models, with average deviations from observational data up to 2–3 °C for the territory in question.

7. Although average deviations from selected models are small, their spatial distributions show local extremes, which reach $-10 \div -12$ °C and $+10 \div +12$ °C.

8. Territorial overestimation of air temperatures by models is connected with mountain conditions and high altitudes of weather stations (up to 1800 m). This should be considered when estimating future temperature projections. Temperature overestimation in the mountains is most significant in summer (up to $+12$ °C) and the least in autumn and winter (up to $+4 \div +6$ °C).

9. Territorial underestimations of temperatures by models occur mainly in the north and west and are caused by two different causes of warming local character: the influence of the Sahara and Sahel from the north and the Gulf of Guinea from the west. These overestimations also have a seasonal course. The largest negative deviations are observed in the spring, the hottest intermonsoon period, and the smallest in the summer and winter monsoon.

References

1. Amraoul, L.: Characterization of the 1970s climatic shift in Northwest Africa. Pub. IAHS **340**, 513–520 (2010).
2. Vissin, E.W.: Impact of climatic variability and surface state dynamics on runoff in the Beninese Niger River Basin, PhD thesis. Hydro climatology. University of Burgundy—Climatology Research Center. CNRS—UMR 5210, version 1, 285 (11 Feb. 2010).
3. Masson-Delmotte, V., P. Zhai, A. Pirani, S. L. Connors, C. Péan, S. Berger, N. Caud, Y. Chen, L. Goldfarb, M. I. Gomis, M. Huang, K. Leitzell, E. Lonnoy, J.B.R. Matthews, T. K. Maycock, T. Waterfield, O. Yelekçi, R. Yu and B. Zhou (eds.). IPCC. Climate Change 2021: The Physical Science Basis. Contribution of Working Group I to the Sixth Assessment Report of the Intergovernmental Panel on Climate Change. Cambridge University Press (2012).
4. Stocker, T.F., Qin, D., Plattner, G.-K., Tignor, M., Allen, S.K., Boschung, J., Nauels, A., Xia, Y., Bex, V., Midgley, P.M.: IPCC. Climate Change 2013: The Physical Science Basis. Contribution of Working Group I to the Fifth Assessment Report of the Intergovernmental Panel on Climate Change/Eds. Cambridge, United Kingdom and New York, NY, USA: Cambridge University Press (2013).
5. Vtoroy otsenochnyy doklad RosGidrometa ob izmeneniyakh klimata i ikh posledstviyakh na territorii Rossiyskoy Federatsii [The second assessment report of RosHydromet on climate change and its consequences on the territory of the Russian Federation]. Moscow, GU VNIIGMI-WDC, 1400 (2018) [In Russian].
6. Bates, B. C., Kundzewicz, Z. W., Wu, S., Palutikof, J. P.: Climate Change and Water, technical paper published by the Intergovernmental Panel on Climate Change. IPCC Secretariat. Geneva, 236 (2008).
7. Acero, F.G., Gracia, J.A., Gallego, M.C.: Peaks-over-threshold study of trends in extreme rainfall over the Iberian Peninsula. Journal of Climate. **24**(4), 1089–1105 (2011).

8. Homar, V., Ramis, C., Romero, R, Alonso, S.: Recent trends in temperature and precipitation over the Balearic Islands (Spain). Climatic Change. **98**, 199–211 (2010).

9. Amraoui, L.: Recent climate evolution in Northwest Africa (Morocco, Mauritania and their near ocean between 1950 and 2008). Thesis of the University Jean Moulin—Lyon III, 43 (2011).

10. Camberlin, P.: Central Africa in the context of tropical interannual and intra-seasonal climate variability, pp. 25–39 (14 Dec 2010). HAL Id: hal-00320705. https://hal.archives-ouvertes.fr/hal-00320705/document

11. Kruger, A. C., Shongwe, S.: Temperature trends in South Africa: 1960–2003. International Journal of Climatology: A Journal of the Royal Meteorological Society. **24**(15), 1929–1945 (2004). https://doi.org/10.1002/joc.1096

12. https://public.wmo.int/en/events/meetings/state-of-climate-africa-2019

13. Diedhiou, A., Bichet, A., Wartenburger, R., Seneviratne, S.I., David, P.: Changes in climate extremes over West and Central Africa at 1.5 °C and 2 °C global warming. Nature. **529**, 477–483 (2018).

14. Hulme, M., Doherty, R., Ngara, T., New, M., Lister, D.: African climate change: 1900–2100. Climate Research. **17**(2), 145–168 (2001).

15. Aguilar, E., Aziz Barry, A., Brunet, M., Ekang, L., Fernandes, A., Massoukina, M., Zhang, X.: Changes in temperature and precipitation extremes in western central Africa, Guinea Conakry, and Zimbabwe, 1955–2006. Journal of Geophysical Research: Atmospheres. **114**(2) (2009).

16. Seneviratne, S. I., Donat, M.G., Pitman, A.J., Knutti, R., Wilby, R. L.: Allowable CO_2 emissions based on regional and impact-related climate targets. Nature. **540**, 564–588 (2016).

17. https://report.ipcc.ch/ar6wg2/pdf/IPCC_AR6_WGII_FinalDraft_Chapter09.pdf

18. Pokam, W., Longandjo, G-N., Moufouma-Okia, T., Wilfran, et al.: Consequences of 1.5 °C and 2 °C global warming levels for temperature and precipitation changes over Central Africa. Environmental Research Letters. **13**(5), 55–81 (2018).

19. Grossman, D.: The Congo rainforest is losing ability to absorb carbon dioxide. That's bad for climate change. (2020) 49. https://rainforestjournalismfund.org/fr/node/20909

20. Zaks, L.: Statisticheskoye otsenivaniye [Statistical estimation]. M.: Statistics. 598 (1976) [In Russian].

21. Rekomendatsii po statisticheskim metodam analiza odnorodnosti prostranstvenno-vremennykh kolebaniy rechnogo stoka L [Recommendations on Statistical Methods for Analyzing the Homogeneity of Spatio-Temporal Fluctuations in River Flow]. Gidrometeoizdat, 78 (1984) [In Russian].

22. Malinin, V.N.: Statisticheskie metody analiza gidrometetorologicheskoy informacii. SPb [Statistical methods for the analysis of hydrometeorological information]. RSHU. 408 (2008) [In Russian].

23. Rekomendatsii po privedeniyu ryadov rechnogo stoka i ikh parametrov k mnogoletnemu periodu [Recommendations for bringing river runoff series and their parameters to a multi-year period]. Leningrad, Gidrometeoizdat, 64 (1979) [In Russian].

24. Lobanov, V.A., Lemeshko, N.A., Zhiltsova, E.L., Gorlova, S.A., Reneva, S.A.: Vosstanovleniye mnogoletnikh ryadov temperatury vozdukha na Yevropeyskoy territorii Rossii [Reconstruction of long-term series of air temperature in the European territory of Russia]. Meteorologiya i gidrologiya [Meteorology and Hydrology]. **2**, 5–14 (2005) [In Russian].

25. Lobanov, V.A., Shadurskiy, A.Ye.: Vydeleniye zon klimaticheskogo riska na territorii Rossii pri sovremennom izmenenii klimata. Monografiya [Identification of climatic risk zones on the territory of Russia under current climate change. Monograph]. St. Petersburg, Russian State Humanitarian University, 123, (2013) [In Russian].

26. Lobanov, V.A., Toshchakova, G.G.: Osobennosti i prichiny sovremennykh klimaticheskikh izmeneniy v Rossii [Features and causes of modern climate change in Russia]. Geographic Bulletin, Perm University, Vol. 38, **3**, 79–89 (2016) [In Russian].

27. Lobanov, V.A., Кirilina, К.S.: Sovremennye i budushie izmeneniya klimata Respubliki Sakha (Yakutiya) [Current and future climate changes in the Republic of Sakha (Yakutia)]. Monograph—St. Petersburg, RSHU, 157 (2019) [In Russian].

28. Shukri, O.A.A., Lobanov, V.A., Khamid, M.S.: Sovremennyi i budushiy klimat Araviyskogo poluostrova [The current and future climate of the Arabian Peninsula]. Monograph—St. Petersburg, RSHU, 190 (2018) [In Russian].
29. Lobanov, V.A., Naurozbayeva, Zh.K.: Vliyaniye izmeneniya klimata na ledovyy rezhim Severnogo Kaspiya [Influence of climate change on the ice regime of the Northern Caspian]. Saint-Petersburg, Publishing House of the Russian State Hydrometeorological University, 140 (2021) [In Russian].
30. Lobanov, V.A.: Lektsii po klimatologii. Chast' 2. Dinamika klimata.Kn.2 [Lectures on climatology. Part 2. Climate dynamics. Book 2]. St. Petersburg, Russian State Hydrometeorological University Press, 377 (2018) [In Russian].
31. Lobanov, V.A.: Uchebnoye posobiye po regional'noy klimatologii [Textbook on regional climatology]. St. Petersburg, Russian State Hydrometeorological University Press, 170 (2020) [In Russian].
32. About the WCRP CMIP5 Multi-Model Dataset Archive at PCMDI: http://www-pcmdi.llnl.gov/ipcc/about_ipcc.php
33. Atmospheric Model Intercomparison Project: http://www-pcmdi.llnl.gov/projects/amip/index.php
34. Gates, W.L., 1992: AMIP: The Atmospheric Model Intercomparison Project. Bull. Amer. Meteor. Soc. **73**, 1962–1970.
35. Taylor, K.E., Stouffer, J R., Meehl, G.A., 2012.: An overview of CMIP5 and experiment design. Bull. American Meteorological Society, 485–498 (April 2012).
36. IPCC Standard Output from Coupled Ocean-Atmosphere GCMs. http://www-pcmdi.llnl.gov/ipcc/standard_output.html#Experiments